J|A|C|S
ARTICLES
Published on Web 12/30/2003

Quantitative Analysis of Conformational Exchange Contributions to $^{1}H-^{15}N$ Multiple-Quantum Relaxation Using Field-Dependent Measurements. Time Scale and Structural Characterization of Exchange in a Calmodulin C-Terminal Domain Mutant

Patrik Lundström and Mikael Akke*

Contribution from the Department of Biophysical Chemistry, Lund University, P.O. Box 124, SE-221 00 Lund, Sweden

Received July 25, 2003; E-mail: mikael.akke@bpc.lu.se

Abstract: Multiple-quantum spin relaxation is a sensitive probe for correlated conformational exchange dynamics on microsecond to millisecond time scales in biomolecules. We measured differential $^{1}H-^{15}N$ multiple-quantum relaxation rates for the backbone amide groups of the E140Q mutant of the C-terminal domain of calmodulin at three static magnetic field strengths. The differential multiple-quantum relaxation rates range between -88.7 and 92.7 s^{-1}, and the mean and standard deviation are 7.0 ± 24 s^{-1}, at a static magnetic field strength of 14.1 T. Together with values of the ^{1}H and ^{15}N chemical shift anisotropies (CSA) determined separately, the field-dependent data enable separation of the different contributions from dipolar−dipolar, CSA−CSA, and conformational exchange cross-correlated relaxation mechanisms to the differential multiple-quantum relaxation rates. The procedure yields precise quantitative information on the dominant conformational exchange contributions observed in this protein. The field-dependent differences between double- and zero-quantum relaxation rates directly benchmark the rates of conformational exchange, showing that these are fast on the chemical shift time scale for the large majority of residues in the protein. Further analysis of the differential $^{1}H-^{15}N$ multiple-quantum relaxation rates using previously determined exchange rate constants and populations, obtained from ^{15}N off-resonance rotating-frame relaxation data, enables extraction of the product of the chemical shift differences between the resonance frequencies of the ^{1}H and ^{15}N spins in the exchanging conformations, $\delta\sigma_H\delta\sigma_N$. Thus, information on the ^{1}H chemical shift differences is obtained, while circumventing complications associated with direct measurements of conformational exchange effects on ^{1}H single-quantum coherences in nondeuterated proteins. The method significantly increases the information content available for structural interpretation of the conformational exchange process, partly because $\delta\sigma_H\delta\sigma_N$ is a signed quantity, and partly because two chemical shifts are probed simultaneously. The present results support the hypothesis that the exchange in the calcium-loaded state of the E140Q mutant involves conformations similar to those of the wild-type apo (closed) and calcium-loaded (open) states.

Introduction

Function is encoded in the structural and dynamical properties of biomolecules. A deep understanding of protein function will be reached only by combined analysis of these properties.[1,2] NMR spin relaxation is a powerful tool for characterizing biomolecular dynamics. Motions on a wide range of time scales may be probed, from the very rapid fluctuations of bond vectors, that take place on pico- to nanosecond time scales, to slower collective motions in the micro- to millisecond regime.[3,4] The latter type of dynamics may be characterized quantitatively using Carr−Purcell−Meiboom−Gill (CPMG) or rotating-frame spin-lock ($T_{1\rho}$) experiments, in which conformational exchange between substates with different chemical shifts is manifested by a dispersion of the transverse relaxation rate as a function of the effective field strength.[5] Ongoing methods development and applications in this area are motivated by the implication that processes such as allosteric transitions and enzymatic catalysis may involve motions on these slower time scales.[6] The majority of studies have monitored the relaxation of single-quantum coherences, most commonly involving ^{15}N or ^{13}C, which report on the chemical shift modulation of a single nuclear spin. The extracted information typically consists of the exchange rate, the relative populations of the different substates, and the chemical shift difference between these. Structural interpretation of chemical shifts is far from straightforward.[7] However, in cases where the extracted chemical shift differences

(1) Kay, L. E. *Nat. Struct. Biol.* **1998**, *5 suppl*, 513−517.
(2) Wand, A. J. *Nat. Struct. Biol.* **2001**, *8*, 926−931.
(3) Palmer, A. G.; Williams, J.; McDermott, A. *J. Phys. Chem.* **1996**, *100*, 13293−13310.
(4) Fischer, M. W. F.; Majumdar, A.; Zuiderweg, E. R. P. *Prog. Nucl. Magn. Reson. Spectrosc.* **1998**, *33*, 207−272.
(5) Palmer, A. G.; Kroenke, C. D.; Loria, J. P. *Methods Enzymol.* **2001**, *339*, 204−238.
(6) Akke, M. *Curr. Opin. Struct. Biol.* **2002**, *12*, 642−647.

10.1021/ja037529r CCC: $27.50

can be compared to differences between chemical shifts observed separately for different states of a highly similar system (e.g., free and ligand-bound states, or different mutants), it may be possible to infer what structural changes are associated with the exchange process.[8−11] Also, measurements of chemical shift differences for sets of different nuclides increase the information content significantly and aid in structural interpretation.[12,13]

During the past few years, relaxation studies of multiple-quantum coherences for characterization of conformational exchange have become increasingly popular.[14−19] Exchange-mediated relaxation of multiple-quantum coherences contains a contribution from correlated chemical shift modulation of the different spins involved.[20,21] Clearly, this provides a complementary and more extensive picture of the protein dynamics. Cross-correlated relaxation of multiple-quantum coherences is also a rich source of structural information, as demonstrated in a large number of applications.[22]

The calcium-saturated E140Q mutant of the C-terminal domain of calmodulin (E140Q-Tr2C) exchanges between conformations that resemble the apo and calcium-saturated states of the wild-type domain (wt-Tr2C), as gauged from the chemical shifts and pattern of NOESY cross-peaks.[9,23] The conformational changes between apo and calcium-saturated wt-Tr2C include extensive repacking of the hydrophobic core, reorientations of the α-helices, and exposure of a hydrophobic surface.[24−27] This conformational switch is essential for binding to a large number of target proteins.[28,29] Off-resonance ^{15}N $T_{1\rho}$ measurements on E140Q-Tr2C have revealed that the average exchange correlation time is $\tau_{ex} = 21$ μs at 28 °C and that the two dominating populations are approximately equal.[10] Because of the sizable exchange contributions to the transverse relaxation rates, E140Q-Tr2C is a good model system for studying the dynamics of large-scale structural transitions in general, as well as the biologically relevant process of calmodulin activation in particular.[8]

In the present study, we characterize further the exchange process connecting the open and closed states by measuring the (signed) product of chemical shift differences between the exchanging conformations for the backbone amide ^1H and ^{15}N spins. The method is based on a combined analysis of results obtained from ^{15}N off-resonance $T_{1\rho}$ experiments[10,30] and measurements of differential multiple-quantum relaxation rates of the backbone amide group.[14] This approach enables extraction of the additional structural information contained in the ^1H chemical shifts, while circumventing complications associated with direct measurements of conformational exchange contributions to the relaxation rates of ^1H single-quantum coherences.[12,13] In the present application, the various contributions to differential multiple-quantum relaxation are separated by determining the field-dependence of the relaxation rates, and by measuring the chemical shift anisotropies of the amide ^1H and ^{15}N spins. Previous reports on differential multiple-quantum relaxation have settled for qualitative evaluations, where the existence of conformational exchange was inferred by comparing the magnitudes of the measured relaxation rates with the maximal values expected for exchange-free relaxation.[14,15,17] The extracted product of chemical shift differences is compared to the values calculated from the observed shift changes between the wild-type protein in the apo and calcium-loaded states. The new experimental results effectively double the amount of information describing the structural changes of the exchange process. In addition, the field-dependent data directly benchmark the exchange process on the chemical shift time scale, showing unequivocally that the exchange is fast for the large majority of residues in E140Q-Tr2C.

Theory

The spin states described by the density operators $2N_xH_x$ and $2N_yH_y$ are linear combinations of double-quantum (DQ) and zero-quantum (ZQ) coherences. Thus, if the DQ and ZQ relaxation rates are not equal, $2N_xH_x$ and $2N_yH_y$ will be partially interconverted during a relaxation delay, T_C. Starting from pure $2N_xH_x$, the ratio of expectation values for $2N_yH_y$ and $2N_xH_x$ will evolve as a function of the difference between the DQ and ZQ relaxation rates, $\Delta R_{MQ} = R_{DQ} - R_{ZQ}$:[14]

$$\frac{\langle 2N_yH_y(T_C)\rangle}{\langle 2N_xH_x(T_C)\rangle} = \tanh\left(\frac{\Delta R_{MQ} T_C}{2}\right) \quad (1)$$

It is readily shown that all active relaxation mechanisms, viz. the cross-correlation between the two chemical shift anisotropy tensors (η_{cc}), the dipolar cross-relaxation (σ_{dd}), the cross-correlated dipolar relaxation with external spins (η_{dd}), and the cross-correlated modulation of the isotropic chemical shifts (η_{ex}), result in different relaxation rates for the DQ and ZQ coherences.[31]

$$\Delta R_{MQ} = R_{DQ} - R_{ZQ} = 2(\eta_{cc} + \eta_{dd} + \sigma_{dd} + \eta_{ex}) \quad (2)$$

where the different terms are given by the expressions below:

$$\eta_{cc} = \frac{4}{9}\gamma_H\gamma_N\Delta\sigma_H\Delta\sigma_N B_0^{\,2} J(0) \quad (3)$$

$$\sigma_{dd} = \frac{1}{8}\left(\frac{\mu_0}{4\pi}\right)^2\left(\frac{\gamma_H\gamma_N\hbar}{r_{HN}^3}\right)^2 [6J(\omega_H + \omega_N) - J(\omega_H - \omega_N)] \quad (4)$$

(7) Xu, X. P.; Case, D. A. *Biopolymers* **2002**, *65*, 408−423.
(8) Malmendal, A.; Evenäs, J.; Forsén, S.; Akke, M. *J. Mol. Biol.* **1999**, *293*, 883−899.
(9) Evenäs, J.; Forsén, S.; Malmendal, A.; Akke, M. *J. Mol. Biol.* **1999**, *289*, 603−617.
(10) Evenäs, J.; Malmendal, A.; Akke, M. *Structure* **2001**, *9*, 185−195.
(11) Volkman, B. F.; Lipson, D.; Wemmer, D. E.; Kern, D. *Science* **2001**, *291*, 2429−2433.
(12) Ishima, R.; Wingfield, P. T.; Stahl, S. J.; Kaufman, J. D.; Torchia, D. A. *J. Am. Chem. Soc.* **1998**, *120*, 10534−10542.
(13) Ishima, R.; Torchia, D. A. *J. Biomol. NMR* **2003**, *25*, 243−248.
(14) Kloiber, K.; Konrat, R. *J. Biomol. NMR* **2000**, *18*, 33−42.
(15) Früh, D.; Tolman, J. R.; Bodenhausen, G.; Zwahlen, C. *J. Am. Chem. Soc.* **2001**, *123*, 4810−4816.
(16) Pervushin, K. *J. Biomol. NMR* **2001**, *20*, 275−285.
(17) Schuler, W.; Kloiber, K.; Matt, T.; Bister, K.; Konrat, R. *Biochemistry* **2001**, *40*, 9596−9604.
(18) Früh, D. *Prog. Nucl. Magn. Reson. Spectrosc.* **2002**, *41*, 305−324.
(19) Wang, C.; Palmer, A. G. *J. Biomol. NMR* **2002**, *24*, 263−268.
(20) Wokaun, A.; Ernst, R. R. *Mol. Phys.* **1978**, *36*, 317−341.
(21) Rance, M. *J. Am. Chem. Soc.* **1988**, *110*, 1973−1974.
(22) Schwalbe, H.; Carlomagno, T.; Hennig, M.; Junker, J.; Reif, B.; Richter, C.; Griesinger, C. *Methods Enzymol.* **2001**, *338*, 35−81.
(23) Evenäs, J.; Thulin, E.; Malmendal, A.; Forsén, S.; Carlström, G. *Biochemistry* **1997**, *36*, 3448−3457.
(24) Chattopadhyaya, R.; Meador, W. E.; Means, A. R.; Quiocho, F. A. *J. Mol. Biol.* **1992**, *228*, 1177−1192.
(25) Finn, B. E.; Evenäs, J.; Drakenberg, T.; Waltho, J. P.; Thulin, E.; Forsén, S. *Nat. Struct. Biol.* **1995**, *2*, 777−783.
(26) Kuboniwa, H.; Tjandra, N.; Grzesiek, S.; Ren, H.; Klee, C. B.; Bax, A. *Nat. Struct. Biol.* **1995**, *2*, 768−776.
(27) Zhang, M.; Tanaka, T.; Ikura, M. *Nat. Struct. Biol.* **1995**, *2*, 758−767.
(28) Vogel, H. J. *Biochem. Cell Biol.* **1994**, *72*, 357−376.
(29) Crivici, A.; Ikura, M. *Annu. Rev. Biophys. Biomol. Struct.* **1995**, *24*, 85−116.
(30) Akke, M.; Palmer, A. G. *J. Am. Chem. Soc.* **1996**, *118*, 911−912.
(31) Tessari, M.; Vuister, G. W. *J. Biomol. NMR* **2000**, *16*, 171−174.

$$\eta_{dd} = \frac{1}{2}\left(\frac{\mu_0}{4\pi}\right)^2 \gamma_H \gamma_N \hbar^2 \sum_i \frac{\gamma_i^2}{r_{Hi}^3 r_{Ni}^3}[2J(0) + 3J(\omega_i)] \quad (5)$$

$$\eta_{ex} = 2p_o p_c \tau_{ex} \gamma_H \gamma_N B_0{}^2 \delta\sigma_H \delta\sigma_N \quad (6)$$

and the spectral density may be modeled as:

$$J(\omega) = \frac{2}{5}\frac{\tau_c}{(1 + \tau_c^2\omega^2)} P_2(\cos\theta) \quad (7)$$

in which γ_i is the gyromagnetic ratio of nucleus i; B_0 is the static magnetic field strength; $\Delta\sigma_i$ is the chemical shift anisotropy (assumed to be axially symmetric); $\delta\sigma_i$ is the difference in isotropic chemical shift of nucleus i between the exchanging substates, the populations of which are denoted p_O and p_C; r_{ij} is the distance between nuclei i and j; τ_{ex} is the exchange correlation time; τ_c is the correlation time for overall rotational diffusion; $P_2(x) = (3x^2 - 1)/2$ is the second-order Legendre polynomial; and θ is the angle between the relevant interaction tensors. Equation 6 is only valid in the fast exchange limit, where η_{ex} is proportional to $B_0{}^2$. In the intermediate exchange regime, η_{ex} is linearly dependent on B_0, and in the slow exchange regime, η_{ex} is independent of B_0.[5,19] Equation 7 applies to a rigid molecule undergoing isotropic rotational diffusion; deviations from the former condition are usually treated using the model-free formalism.[32−34] Because all relaxation mechanisms described by eqs 3−6 are predicted to cause differential multiple-quantum relaxation, the effect should be readily detectable, unless cancellation of terms occurs as a consequence of the different field dependence of the various mechanisms.

Material and Methods

NMR Spectroscopy. The sample consisted of uniformly ^{15}N-labeled E140Q-Tr2C at a concentration of 2.0 mM and 16 equiv of Ca^{2+} at pH 6.0 (unbuffered solution). The ^{1}H and ^{15}N assignments have been reported previously.[23,35] The differential multiple-quantum relaxation experiment was performed essentially as reported.[14] Briefly, the spin state $2N_xH_x$ is created using a modified INEPT sequence.[36] In the middle of the subsequent relaxation delay of duration T_C, simultaneous 180° pulses on ^{15}N and ^{1}H are applied to refocus chemical shift evolution and scalar couplings to remote spins. At the end of the relaxation delay, either the $2N_xH_x$ operator ("reference" experiment) or the $2N_yH_y$ operator ("cross" experiment) is converted into longitudinal magnetization. The rest of the experiment encodes the ^{15}N resonance frequencies during the indirect evolution period and subsequently transfers magnetization back to protons for detection. All experiments were performed on Varian Unity INOVA spectrometers at static magnetic field strengths of 11.7, 14.1, and 18.8 T, and a temperature of 28 ± 0.1 °C. In the experiments recorded at 11.7 and 14.1 T, the proton 180° pulse in the middle of the relaxation delay was implemented as a RE-BURP pulse[37] centered at 8.5 ppm, which provides 98% inversion over the amide range. The experiment performed at 18.8 T employed a nonselective proton 180° pulse during the relaxation delay; that is, the scalar coupling to H^α was not refocused. In this case, eqs 1 and 8 are valid only in the limit that T_C approaches zero. Accordingly, this data set was fitted with a second-order polynomial, the (negative) slope of which at $T_C = 0$ yields $\Delta R_{MQ}/2$. The robustness of this approach was verified by comparing a similarly recorded data set at 11.7 T with the one recorded using a selective RE-BURP pulse; these two data sets yielded indistinguishable results (not shown). Decoupling of the ^{15}N spins during acquisition was performed using the GARP sequence[38] with a field-strength of 1.0 kHz. Reference and cross experiments were recorded with relaxation delays of 10, 20, 30, 40, and 50 ms at all three values of B_0.

NMR Data Processing and Analysis. All data were processed using nmrPipe.[39] Two apodization schemes were employed to enhance either sensitivity or resolution. The former scheme used exponential and cosine-bell apodization in t_2 and t_1, respectively, while the latter used a Lorentzian−Gaussian window function in t_2, and linear prediction to 256 points followed by a cosine bell in t_1. The final size of each matrix was 1024 × 1024 real points after zero filling and Fourier transformation. Peak intensities were evaluated as peak heights. The uncertainty of the peak heights was estimated as the standard deviation of the baseline noise. The intensity ratio between the cross and reference experiments was evaluated for all relaxation delays.

It should be noted that the reference and cross spectra are out of phase by 180° if performed as described[14] on a Varian INOVA spectrometer. In experiments involving nuclides with gyromagnetic ratios of different signs, the implementation of RF phases is not consistent with the definition usually assumed in spin dynamics calculations.[40] This has the practical consequence that for nuclei with positive gyromagnetic ratios, an RF-pulse with phase "y" (according to the phase table of the pulse sequence) in reality is delivered with phase "$-y$", and vice versa, while all other pulses have the expected phases (as given in the phase table). In the present case, this implies that the reference experiment corresponds to $\langle -2N_xH_x\rangle$ rather than $\langle 2N_xH_x\rangle$ (assuming that $\langle 2N_yH_y\rangle$ is measured in the cross experiment). Taking these considerations into account, the appropriate expression to fit against the experimental data is thus

$$I_{cc}(T_C)/I_{ref}(T_C) = \tanh(-\Delta R_{MQ} T_C/2) \quad (8)$$

in which $I_{cc}(T_C)$ and $I_{ref}(T_C)$ are the intensities at time T_C of the cross and reference experiments, respectively. This treatment ensures that the signs of the extracted relaxation rates of eqs 3−6 will be correct. Errors in the fitted parameters were estimated by Monte Carlo simulations.[41]

Chemical Shift Calculations. Ring-current shifts of the amide ^{1}H resonance frequencies were calculated using SHIFTS v4.1[42,43] and were based on the NMR structure ensembles of apo and calcium-loaded wt-Tr2C.[25] The average difference in ring-current shifts between apo and calcium-loaded wt-Tr2C was calculated using 20 structures of each ensemble.

Hydrogen Bond Calculations. Hydrogen bonds involving the backbone amide groups were calculated from structures of the apo and calcium-loaded wild-type protein (PDB entries 1CLL,[24] 1CMF,[25] and 1CFC[26]) using MOLMOL,[44] with distance and angle cutoffs of 2.4 Å and 35°, respectively.

Results and Discussion

We have measured the difference in relaxation rates of DQ and ZQ coherences of the backbone amide ^{1}H and ^{15}N spins in

(32) Lipari, G.; Szabo, A. *Biochemistry* **1981**, *20*, 6250−6256.
(33) Lipari, G.; Szabo, A. *J. Am. Chem. Soc.* **1982**, *104*, 4546−4559.
(34) Clore, G. M.; Szabo, A.; Bax, A.; Kay, L. E.; Driscoll, P. C.; Gronenborn, A. M. *J. Am. Chem. Soc.* **1990**, *112*, 4989−4991.
(35) Evenäs, J.; Malmendal, A.; Thulin, E.; Carlström, G.; Forsén, S. *Biochemistry* **1998**, *37*, 13744−13754.
(36) Morris, G. A.; Freeman, R. *J. Am. Chem. Soc.* **1979**, *101*, 760−762.
(37) Geen, H.; Freeman, R. *J. Magn. Reson.* **1991**, *93*, 93−141.
(38) Shaka, A. J.; Barker, P. B.; Freeman, R. *J. Magn. Reson.* **1985**, *64*, 547−552.
(39) Delaglio, F.; Grzesiek, S.; Vuister, G. W.; Zhu, G.; Pfeifer, J.; Bax, A. *J. Biomol. NMR* **1995**, *6*, 277−293.
(40) Levitt, M. H. *J. Magn. Reson.* **1997**, *126*, 164−182.
(41) Press, W. H.; Flannery, B. P.; Teukolsky, S. A.; Vetterling, W. T. *Numerical Recipes. The Art of Scientific Computing*; Cambridge University Press: Cambridge, 1986.
(42) Ösapay, K.; Case, D. A. *J. Biomol. NMR* **1994**, *4*, 215−230.
(43) Xu, X. P.; Case, D. A. *J. Biomol. NMR* **2001**, *21*, 321−333.
(44) Koradi, R.; Billeter, M.; Wüthrich, K. *J. Mol. Graphics* **1996**, *14*, 51−55.

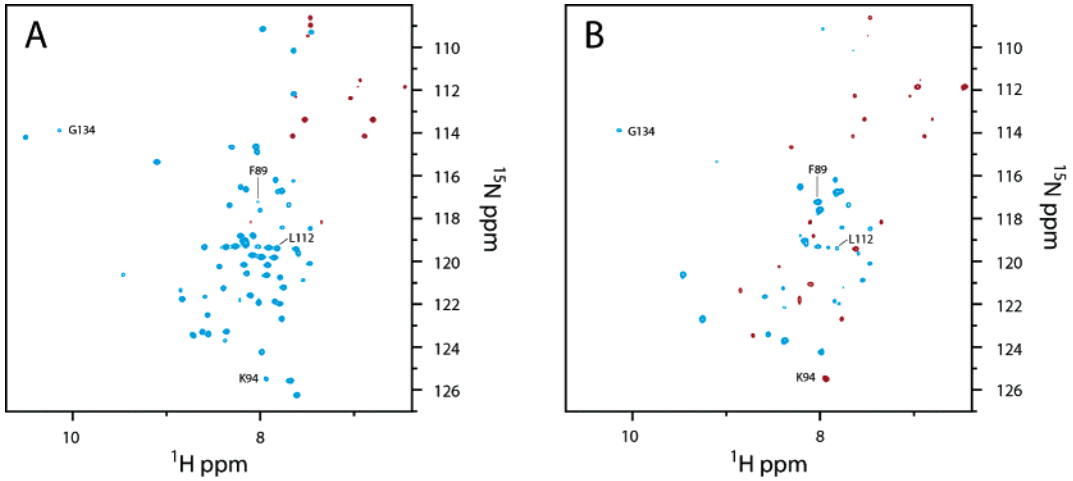

Figure 1. Representative spectra for (A) the reference and (B) the cross experiments. Red contour levels indicate negative intensities, and blue contours indicate positive intensities. For clarity, peak intensities in the cross spectrum have been scaled by a factor of 8 relative to those in the reference spectrum.

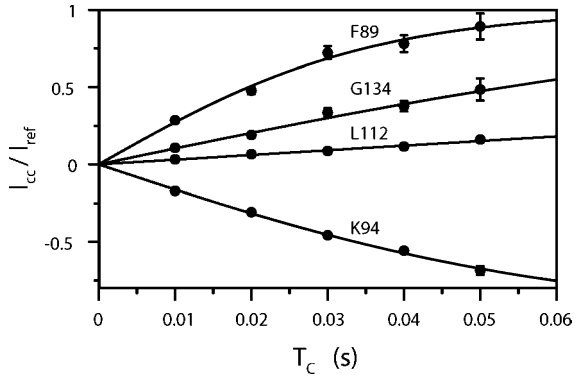

Figure 2. Representative build-up curves following the function $\langle I_{cc}\rangle/\langle I_{ref}\rangle = \tanh(-\Delta R_{MQ}T_C/2)$ for residues F89, K94, L112, and G134 at 14.1 T. The fitted values of ΔR_{MQ} are 50 ± 1, -31.5 ± 0.1, 6.10 ± 0.07, and 20.9 ± 0.6 s^{-1}, respectively.

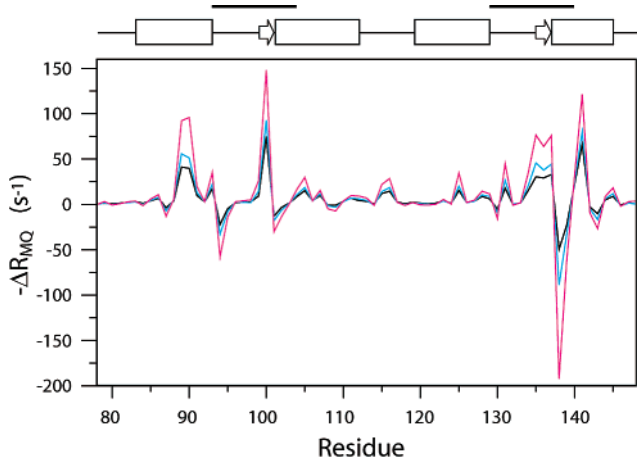

Figure 3. Differential multiple-quantum relaxation rates, ΔR_{MQ}, for E140Q-Tr2C at 11.7 T (black), 14.1 T (cyan), and 18.8 T (magenta). The structural elements and calcium-binding loops of the protein are indicated above the graph.

E140Q-Tr2C at 28 °C. Representative reference and cross-relaxation spectra are shown in Figure 1. The resonances of the N-terminal residues M76 and K77 were not observed in the spectra, presumably due to fast amide proton exchange with the solvent. Extraction of data was not possible for N97 and Q140 because of resonance overlap. For the remaining 69 residues, the difference in relaxation rate constants between DQ and ZQ coherences (ΔR_{MQ}) was obtained from the build-up curves, as described by eq 8 and exemplified in Figure 2. No attenuation of the intensity ratios due to amide proton exchange with solvent was observed at longer relaxation delays, in agreement with numerical calculations based on measured amide proton exchange rates (not shown). Figures 2 and 3 reveal a wide distribution of ΔR_{MQ} with both positive and negative values. Figure 3 displays ΔR_{MQ} obtained at each of the three static magnetic field strengths, plotted against the amino acid residue number. The mean values of ΔR_{MQ} are -6.2 ± 17, -7.0 ± 24, and -9.9 ± 42 s^{-1} at 11.7, 14.1, and 18.8 T, respectively. The largest magnitudes of ΔR_{MQ} are found in the two calcium-binding loops, corresponding to residues 93−104 and 129−140, and for residues F89, R90, and F141.

In the absence of conformational exchange, ΔR_{MQ} results from the balance of the dipolar (η_{dd} and σ_{dd}) and CSA (η_{cc}) contributions. As is evident from eq 4, the contribution to ΔR_{MQ} from dipolar cross-relaxation (σ_{dd}) is positive but small, due to its dependence on high-frequency spectral densities only. The contribution from correlated dipolar interactions with remote protons (η_{dd}) is always negative (eqs 5 and 7; note that a negative value of $P_2(\cos\theta)$ would require that the remote spin i is closer to both the amide nitrogen and the proton than $1.09r_{HN}$, which is physically impossible). The relaxation caused by the interaction between the ^1H and ^{15}N CSA tensors (η_{cc}) is field-dependent, but always leads to faster relaxation of DQ than ZQ coherences, as can be seen from eq 3 using expected values of $\Delta\sigma_N$, $\Delta\sigma_H$, and θ.[45−49] The dipolar contributions may be estimated on the basis of a structural model of the protein, together with values of $J(\omega)$ at the relevant frequencies. Likewise, the CSA contribution may be calculated on the basis of measured values of $\Delta\sigma_N$ and $\Delta\sigma_H$, together with $J(\omega)$. Approximate calculations using the measured correlation time for rotational diffusion at 28 °C, $\tau_c = 4.2$ ns, predict that the dipolar and CSA contributions nearly cancel at the static

(45) Tjandra, N.; Szabo, A.; Bax, A. *J. Am. Chem. Soc.* **1996**, *118*, 6986−6991.
(46) Tjandra, N.; Bax, A. *J. Am. Chem. Soc.* **1997**, *119*, 8076−8082.
(47) Tessari, M.; Mulder, F. A. A.; Boelens, R.; Vuister, G. W. *J. Magn. Reson.* **1997**, *127*, 128−133.
(48) Fushman, D.; Tjandra, N.; Cowburn, D. *J. Am. Chem. Soc.* **1998**, *120*, 10947−10952.
(49) Kroenke, C. D.; Rance, M.; Palmer, A. G. *J. Am. Chem. Soc.* **1999**, *121*, 10119−10125.

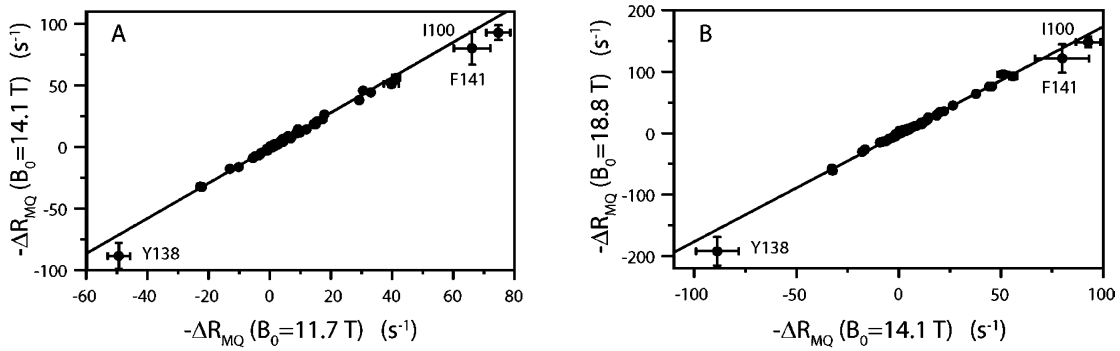

Figure 4. Differential multiple-quantum relaxation rates, ΔR_{MQ}, (A) measured at 14.1 T plotted against data at 11.7 T. The equation of the fitted line is $y = -0.96 + 1.43x$. (B) ΔR_{MQ} measured at 18.8 T plotted against data at 14.1 T. The equation of the fitted line is $y = -1.7 + 1.75x$.

magnetic field strengths employed here. Chemical exchange is thus the only mechanism that can account for the wide range of ΔR_{MQ} values observed for E140Q-Tr2C (Figures 2 and 3). Equation 6 shows that the conformational exchange rate (η_{ex}) may be negative or positive, depending on whether the isotropic chemical shift changes of the two nuclei are correlated or anti-correlated. The observation of negative values of ΔR_{MQ} thus directly reveals anti-correlated modulation of the amide ^{1}H and ^{15}N chemical shifts during the exchange process for a subset of residues in E140Q-Tr2C.

The Conformational Exchange Is Fast on the Chemical Shift Time Scale. Using ΔR_{MQ} data obtained at multiple static magnetic field strengths, it is possible to separate η_{dd} from η_{cc} and η_{ex}, provided that the latter is intermediate to fast on the chemical shift time scale (such that it depends on B_0). Figure 4 shows the data from the different fields plotted against each other, with the straight lines indicating linear least-squares fits that take into account errors in both dimensions.[41] In the case of fast conformational exchange and equal contributions from the field-independent terms (η_{dd} and σ_{dd}) for all residues, the expected slope of the lines should scale quadratically with the ratio of the two fields. The fitted lines have slopes of 1.43 ± 0.01 (plotting 14.1 T versus 11.7 T) and 1.75 ± 0.01 (18.8 T versus 14.1 T). Comparing these results to the theoretical values of 1.44 and 1.78, we conclude that the process is in the fast exchange limit at all three values of B_0 for the large majority of residues. Residues I100, Y138, and F141, which have the largest magnitudes of ΔR_{MQ}, are the ones most likely not to be in fast exchange. The data for these residues fall outside of the 95% prediction interval obtained by linear regression that excludes these outliers.[50]

Cross-Correlated Dipole−Dipole Relaxation. Given that conformational exchange is fast, linear regression of ΔR_{MQ} versus B_0^2 for each residue yields the dipolar cross-correlation contribution to ΔR_{MQ} as the intercept (Figure 5). This approach safely neglects the contributions from high-frequency spectral densities to η_{dd}, cf. eq 5, which amount to 1.5% of ΔR_{MQ} (at $B_0 = 14.1$ T). Similarly, the cross-relaxation (σ_{dd}) between the ^{15}N and ^{1}H spins can be neglected, because $\langle\sigma_{dd}\rangle = 0.06 \pm 0.02$ s^{-1},[9] corresponding to 5% of the total dipolar relaxation ($\eta_{dd} + \sigma_{dd}$) in the present experiment. Residues I100, Y138, and F141 have unreasonably large values of η_{dd} (Figure 6a), which may again imply that they are outside the fast exchange limit. Excluding these three residues, the average contribution

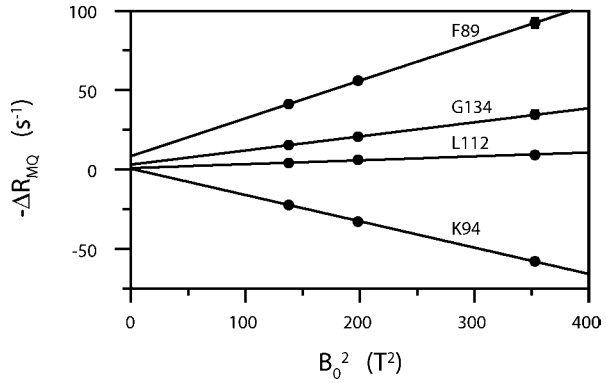

Figure 5. Differential multiple-quantum relaxation rates, ΔR_{MQ}, plotted as a function of the static magnetic field strength squared, B_0^2. Representative data are shown for residues F89, K94, L112, and G134. The intercept corresponds to the dipolar contribution (η_{dd}) to ΔR_{MQ}, while the slope corresponds to the sum of the contributions from the CSA−CSA cross-correlation (η_{cc}) and correlated chemical shift modulation (η_{ex}). The fitted intercepts are 5.7 ± 2, 1.2 ± 0.5, 1.6 ± 0.2, and 2.3 ± 0.9 s^{-1} for residues F89, K94, L112, and G134, respectively, and the slopes are 0.23 ± 0.01, −0.170 ± 0.005, 0.025 ± 0.001, and 0.09 ± 0.01 s^{-1} T^{-2}, respectively.

from dipolar cross-correlation is $\langle\eta_{dd}\rangle = -1.2 \pm 2.0$ s^{-1}. The density of remote spins surrounding the amide group dominates the variability of the dipolar contribution, making it mainly a structural probe. The mean value is approximately 50% lower than that predicted (−2.2 ± 0.5 s^{-1}) from population-weighted (1:1) calculations based on internuclear distances measured in the apo and calcium-loaded wt-Tr2C structures,[25] together with experimentally determined values of $J(\omega)$ (Figure 6a).[9] However, the predicted and measured values of $\langle\eta_{dd}\rangle$ agree within experimental errors, which are relatively large due to extrapolation.

Cross-Correlated CSA−CSA Relaxation. In the fast exchange limit, the CSA and exchange contributions cannot be separated by their dependence on B_0 (cf., eqs 3 and 6). However, the CSA contribution may be calculated accurately if $\Delta\sigma_N$, $\Delta\sigma_H$, and the angle θ between the two tensors are known. In contrast to the case for the ^{15}N CSA,[49] the amide ^{1}H CSA exhibits considerable variability that depends primarily on the hydrogen bond length[46] and ring-current shifts;[51] the mean values reported for α-helices and β-strands are 7.2 and 11.2 ppm, respectively.[46] We measured the amide ^{1}H CSA using the method proposed by Tessari et al.[47] (data not shown). Using these data, together with previously determined ^{15}N CSA values and spectral densities,[9] we calculated the CSA contribution to ΔR_{MQ} (Figure

(50) Devore, J. L. *Probability and Statistics for Engineering and the Sciences*, 5th ed.; Brooks/Cole Publishing Company: Monterey, 1999.

(51) Boyd, J.; Skrynnikov, N. R. *J. Am. Chem. Soc.* **2002**, *124*, 1832−1833.

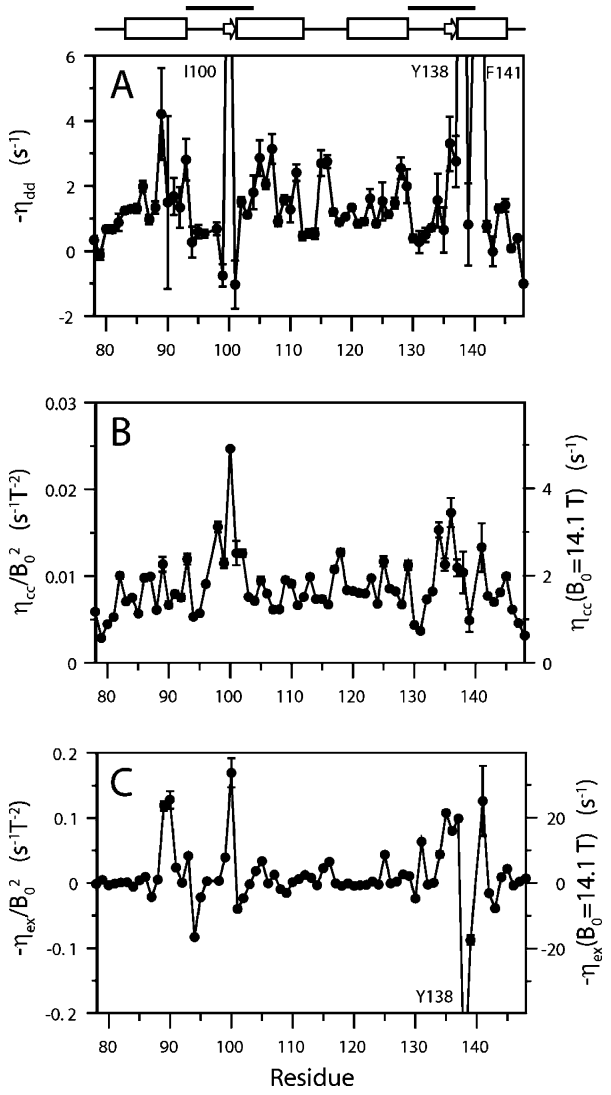

Figure 6. The different contributions to ΔR_{MQ} plotted versus residue number: (A) η_{dd}, dipole−dipole cross-correlation relaxation rate; (B) η_{cc}, CSA−CSA cross-correlation relaxation rate; (C) η_{ex}, exchange rate due to correlated modulation of the ^{15}N and ^1H isotropic chemical shifts. The structural elements and calcium-binding loops of the protein are indicated above the graphs.

6b). For residues that are not involved in conformational exchange, the slope of the fitted line in Figure 5 directly corresponds to the CSA contribution. However, the sensitivity of the measurement is in general poor for these cases, because η_{dd} and η_{cc} have opposite signs and are approximately equal in magnitude, as noted above. The calculated mean value of the CSA−CSA contribution is $\langle\eta_{cc}\rangle/B_0^2 = (8.7 \pm 3.5) \times 10^{-3}\ s^{-1}\ T^{-2}$, corresponding to $1.7 \pm 0.7\ s^{-1}$ at 14.1 T. The variation in the CSA-mediated relaxation depends primarily on the ^1H CSA, which in turn depends on structural factors, most notably the hydrogen bond length. As a result, the CSA−CSA cross-correlation is expected to yield higher values of ΔR_{MQ} for residues in β-sheet structures than for those in α-helical conformation.[46,52] The highest values of η_{cc} in E140Q-Tr2C are observed for I100 and V136, which are the central residues in the short β-sheet (Figure 6b). Also, the surrounding residues show larger than average values of η_{cc}, indicating that they are in an extended conformation, as observed in the solution structures of wt-Tr2C.[25] However, the η_{cc} data are scattered, precluding extraction of any conclusive structural information from these data alone. This is consistent with the observations by Tessari and Vuister,[31] who could measure η_{cc} directly from the field-dependence of ΔR_{MQ}, because chemical exchange was insignificant in that system.

Cross-Correlated Chemical Shift Modulation. In the present case, the most interesting information lies in the exchange contribution. The slope of the fitted line in Figure 5 yields η_{ex} following subtraction of the CSA contribution. With a mean magnitude of $\langle|\eta_{ex}|\rangle/B_0^2 = 0.03 \pm 0.05\ s^{-1}\ T^{-2}$, corresponding to $6 \pm 10\ s^{-1}$ at 14.1 T, η_{ex} is the dominant contribution to ΔR_{MQ} for the majority of residues even at 11.7 T (Figure 6c). Thus, η_{ex} is more accurately determined than the other contributions and can be used reliably to extract information on the conformational exchange process. Residues with large magnitudes of η_{ex} are clustered in the amino acid sequence (Figure 6c). The two calcium-binding loops (residues 93−104 and 129−140), together with residues F89, R90, and F141, exhibit particularly high values of $|\eta_{ex}|$. Figure 7 shows the values of $|\eta_{ex}|$ color coded onto the wild-type apo and calcium-saturated structures of Tr2C. It is evident from Figure 7 that residues with large values of $|\eta_{ex}|$ cluster also in space.

Extracted Chemical Shift Differences. Provided that the exchange correlation times and populations of the two exchanging conformations are known, it is possible to extract the product of the chemical shift differences ($\delta\sigma_N\delta\sigma_H$) between the two conformations, using eq 6. Exchange correlation times and populations have been determined previously for 43 residues in E140Q-Tr2C, using ^{15}N off-resonance $T_{1\rho}$-experiments.[10] In principle, the correlation time for modulation of a single ^{15}N chemical shift could be different from that for correlated modulation of the ^1H and ^{15}N chemical shifts. However, because the two nuclei are covalently linked, we expect that τ_{ex} determined for ^{15}N should provide an excellent approximation. The weighted mean values are $\langle\tau_{ex}\rangle = 21 \pm 3\ \mu s$, with a range of 13−46 μs, and $\langle p_O\rangle = 0.5 \pm 0.17$.[10] The populations are less well determined than the exchange correlation times. However, the product $p_O p_C = p_O(1 - p_O)$ varies by less than 12% within the range given by the relative error (34%) of the estimated mean population, and the average value can be used for all residues. In contrast, the variability in τ_{ex} has a larger effect on the extracted chemical shift differences, even though the statistical site-to-site variability is relatively small.[10] Using the average population and either the residue-specific exchange times, for those residues where this value is available, or the average exchange time, for those residues where it is not, we calculated the product $\delta\sigma_N\delta\sigma_H$ from the ΔR_{MQ} results for 69 residues. In Figure 8, $\delta\sigma_N\delta\sigma_H$ extracted from the ΔR_{MQ} data are superimposed on the values calculated from the chemical shift differences between the apo and calcium-saturated states of wt-Tr2C.[25] The linear correlation coefficient for the two data sets was evaluated for the different segments: helix E, $r = 0.69$ (10 residues); helix F, $r = 0.47$ (11); helix G, $r = 0.57$ (10); helix H, $r = 0.71$ (10); loop III, $r = 0.83$ (8); loop IV, $r = -0.07$ (9); linker, $r = 0.94$ (6); and all residues, $r = 0.57$ (69).

As discussed above, $\delta\sigma_N\delta\sigma_H$ may be positive or negative, depending on whether the chemical shift changes of the two nuclei are correlated or anti-correlated. The sign of $\delta\sigma_N\delta\sigma_H$

(52) Tessari, M.; Vis, H.; Boelens, R.; Kaptain, R.; Vuister, G. W. *J. Am. Chem. Soc.* **1997**, *119*, 8985−8990.

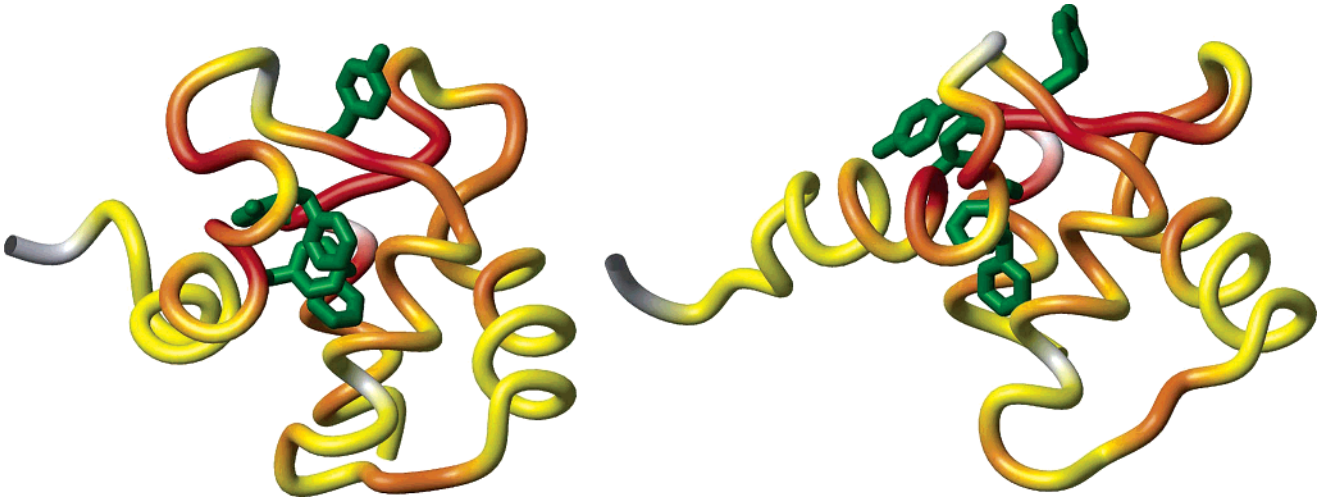

Figure 7. Magnitudes of the correlated chemical shift modulation, $|\eta_{ex}|$, color coded onto the structures of the apo and calcium-loaded states of wt-Tr2C (PDB entries 1cmf and 1cmg, respectively[25]). The color scale ranges continuously from yellow to red, corresponding to $|\eta_{ex}| < 2\ s^{-1}$ and $|\eta_{ex}| > 32\ s^{-1}$ at 14.1 T. Residues for which data were not obtained are shown in gray. The side chains of the aromatic residues (F89, F92, Y99, Y138, and F141) are shown in green. The figure was prepared using MOLMOL.[44]

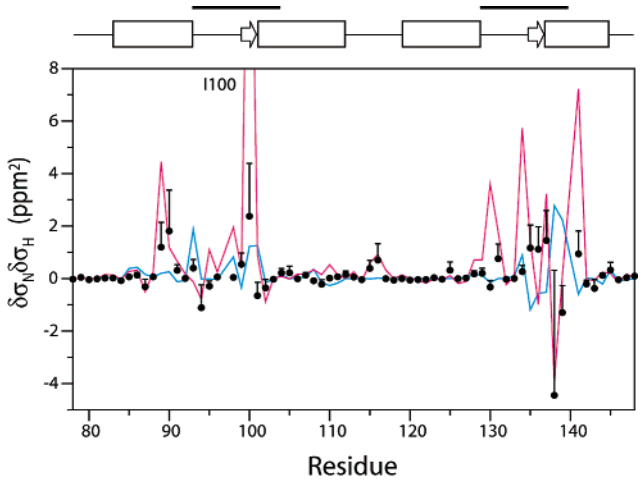

Figure 8. Extracted values of $\delta\sigma_N\delta\sigma_H$, obtained from η_{ex} and previously determined values of τ_{ex} and p_O,[10] plotted versus residue number. Filled circles indicate experimental values of $\delta\sigma_N\delta\sigma_H$ obtained for E140Q-Tr2C. The continuous line in magenta connects the values of $\delta\sigma_N\delta\sigma_H$ calculated from the measured chemical shifts of the apo and calcium-loaded states of wt-Tr2C.[9,25] The continuous line in cyan represents $\delta\sigma_N\delta\sigma_H$ calculated as the ring-current contribution to $\delta\sigma_H$ (see the text for details), multiplied with the measured $\delta\sigma_N$ between the apo and calcium-loaded states of wt-Tr2C. For clarity, $\delta\sigma_N\delta\sigma_H$ for I100 of wt-Tr2C (21 ppm^2) is not shown. The structural elements and calcium-binding loops of the protein are indicated above the graph.

obtained for E140Q-Tr2C agrees with the wild-type data for 50 residues, while 19 residues differ in sign. However, the magnitude of $\delta\sigma_N\delta\sigma_H$ is small for the large majority of cases that deviate; the set of such residues with $\delta\sigma_N\delta\sigma_H > 0.3$ ppm^2 is limited to S101, V108, I130, and V136. The correspondence of the sign of $\delta\sigma_N\delta\sigma_H$ is a critical piece of evidence that the protein is exchanging between conformations that closely resemble the apo and calcium-loaded states of wt-Tr2C.

For several residues located in the calcium-binding sites (residues 93−104 and 129−140), the observed values of $\delta\sigma_N\delta\sigma_H$ agree poorly with those calculated from the measured wild-type protein shifts (Figure 8). Key examples are those backbone amides that exhibit Ca^{2+}-dependent hydrogen bond formation to Ca^{2+}-ligating side chains: D95 is hydrogen bonded to the side chain of E104, G98 is hydrogen bonded to D93, S101 to E104, I130 to E140, and G134 to D129; in addition, F141 is hydrogen bonded to the backbone carbonyl group of N137 in the calcium-loaded state, but not in the apo state. In contrast, reasonably good agreement is observed for a number of residues with smaller chemical shift differences: A102, A103, G132, D133, none of which is hydrogen bonded in either the apo or calcium-loaded states, and also for residues K94, G96, and Y99, which are hydrogen bonded in both states. These observations (agreements and disagreements alike) indicate that the hydrogen bonding patterns in the calcium-binding loops of E140Q-Tr2C remain largely intact during the exchange, which may be expected, because E140Q-Tr2C is 98% calcium saturated under the present experimental conditions. Thus, the present results provide further evidence that the exchange contributions to relaxation in E140Q-Tr2C are not caused primarily by chemical exchange of the calcium ions in and out of the binding sites, in agreement with previous conclusions.[9,10] Residues Q135-E139 provide counterexamples where $\delta\sigma_N\delta\sigma_H$ agrees relatively well with the wild-type value. A possible interpretation is that this part of the calcium-binding loop fluctuates between conformations with Ca^{2+}-coordination and hydrogen bonds similar to those in the apo and calcium-loaded wild-type protein. Such a local destabilization may be explained by the mutation E140Q, which perturbs both the Ca^{2+}-coordination and the hydrogen bonding pattern in this part of the loop. This interpretation mirrors what has previously been suggested on the basis of the ^{15}N chemical shift differences of I100 and V136,[10] both of which show significant differences from the wild-type $\delta\sigma_N\delta\sigma_H$. We emphasize that the detailed structures of E140Q-Tr2C have not yet been determined and that there may well be additional differences as compared to wt-Tr2C.

For comparison, Figure 8 includes values of $\delta\sigma_N\delta\sigma_H$ calculated as the ring-current contribution to $\delta\sigma_H$, multiplied by the measured $\delta\sigma_N$ between the apo and calcium-loaded states of wt-Tr2C. Clearly, ring-current effects provide a dominant contribution to the chemical shift changes for a subset of the amide protons, whereas for other residues additional contributions are clearly important. Inspection of the wild-type structures indicates that, outside of the calcium-binding loops, these

additional contributions are associated with local changes in helical structure (e.g., between 3_{10} and α). The experimental $\delta\sigma_N\delta\sigma_H$ agrees well with what is expected on the basis of ring-current shifts for several residues in the calcium-binding loops, including A128-I130.

Taken together, the present results suggest that the global conformational exchange, including repacking of the hydrophobic core (Figure 7), in E140Q-Tr2C is similar to the structural change observed between apo and calcium-loaded wt-Tr2C. The current results provide important new information on the exchange process that goes beyond what was previously known from ^{15}N relaxation alone.[9,10]

Conclusions

Measurement of the static magnetic field dependence of $^1H-^{15}N$ differential multiple-quantum relaxation rates, together with the CSA of the two nuclei, enable quantitative evaluation of the conformational exchange contributions to the differential relaxation rates and provide an assessment of the time scale of the exchange process. Combined analysis of differential $^1H-^{15}N$ multiple-quantum relaxation rates and ^{15}N relaxation dispersion should be of general use for extracting ^1H and ^{15}N chemical shift differences between exchanging states, which add valuable information on the structural change of exchange processes. In combination with published methods to derive the sign of $\delta\sigma_N$,[53] the present method enables extraction of both the magnitude and the sign of $\delta\sigma_H$. In the case of E140Q-Tr2C, the new data strongly support the notion that the protein exchanges between two major conformations that are similar to the apo and calcium-saturated forms of the wild-type protein. The static magnetic field dependence of the differential multiple-quantum relaxation rates directly shows that the conformational exchange is fast on the chemical shift time scale for the large majority of residues. The present study illustrates the power of using a combination of different relaxation methods to probe protein dynamics.

Acknowledgment. This work was supported by the Swedish Research Council and the Swedish Foundation for Strategic Research (individual grant to M.A.). The NMR experiments were performed at the Swedish NMR Center at Göteborg University, with the expert assistance of Charlotta Damberg. We thank Frans Mulder for helpful discussions.

JA037529R

(53) Skrynnikov, N. R.; Dahlquist, F. W.; Kay, L. E. *J. Am. Chem. Soc.* **2002**, *124*, 12352−12360.